Substitution of Er, In, and Hf in $LiNbO_3$: Evidence for multiple defect distributions about dopant sites

C. Mackeen,[1] F. Bridges,[1,*] L. Kovács,[2] and J. Castillo-Torres[3]
[1]*Physics Department, University of California, Santa Cruz, California 95064, USA*
[2]*Institute for Solid State Physics and Optics, Wigner Research Center for Physics, Budapest, Hungary*
[3]*Departamento de Física y Matemáticas, Universidad Iberoamericana, Prolongación Paseo de la Reforma 880, México D. F. 01219, México*

(Received 26 February 2018; revised manuscript received 12 June 2018; published 6 September 2018)

Many dopants are incorporated into $LiNbO_3$ (LNO) to modify the physical properties, particularly many optical properties. To understand these changes, the substitution site for the dopant must be known. Here we provide a detailed EXAFS study of the local environment about the metal (M) ion dopants indium, erbium, and hafnium in LNO, using crystals grown in both stoichiometric and congruent forms. In primarily substitutes at the Li site in congruent material; Er also substitutes mostly on the Li site with a small fraction roughly 10% on the Nb site—the substitution sites for Er do not appear to change much between stoichiometric and congruent LNO. For Hf, approximately half the dopant substitutes on Li and half on Nb. In all cases, some charge compensating defects are required (self-compensating schemes are not consistent with the data), and can occupy several nearby sites in the crystal leading to many slightly different distributions, some of which may be metastable. For each dopant, changes in the the M-O shell approximately follow the ionic radius of the dopant ion; in addition, the Nb neighbors about M on a Li site are shifted away from the dopant, with large displacements for some dopants such as Er. Comparisons with other experiments and existing calculations are discussed.

DOI: 10.1103/PhysRevMaterials.2.093602

I. INTRODUCTION

$LiNbO_3$ (LNO) has a range of very interesting behaviors [1–4], including in particular a number of important nonlinear optical properties [5–8] such as photorefraction and second harmonic generation, which lead to a range of applications. In addition, LNO materials can be grown in two different forms—congruent LNO (cLNO, approximately $Li_{0.95}Nb_{1.01}O_3$) and stoichiometric LNO (sLNO), which can have significantly different properties [7,9]; however the composition can vary between these two cases. For harmonic generation, the photorefractive effect needs to be suppressed to reduce optical damage when high light intensity is used [10,11]; this is achieved in LNO by adding dopants such as Mg, Zn, In, etc. Recently Hf at concentrations above 3 mol % [8] also greatly reduces the optical damage. For optical waveguide applications, Ti^{4+} is added—often via diffusion at high T (1100 °C, 50 h), to improve the performance [12,13], while Fe [12,13] and Bi [14,15] at low concentrations improve the photorefraction index [6]. In the last decade there are also a large number of papers on codoped LNO (two or more dopants) in which the doubly or triply doped materials have improved properties. However for most systems, there is little direct evidence as to the substitution site for a defect, and there is some evidence that there may be different configurations for a given dopant (different site occupations and/or different distributions of charge compensating defects) that lead to slightly different properties, as for $LiNbO_3$:Ti [12]. Here "defect" can refer to vacancies (e.g., a Li vacancy, V_{Li}), a dopant atom on a metal site (e.g., In on a Li site, In_{Li}), or antisite defects (e.g., Nb on a Li site, Nb_{Li}).

Consequently a very important characterization of doped LNO is the site occupation of a range of dopants with different valences in both sLNO and cLNO. Such information is needed for modeling how dopants modify the optical properties. In general the dopants used have a different valence from Li^+ and Nb^{5+} and open questions remain as to which site(s) the dopant occupies, does the substitution site change with concentration or sample growth, and where the charge compensating defects are located.

Recently we have shown that for Zn dopants, the primary substitution site is on Li, i.e., Zn_{Li}, for both cLNO and sLNO; at most a few percent of Zn is on an Nb site [16,17]. Since Zn has a 2+ valence this requires Li vacancies for charge compensation. There are a few theoretical calculations for the solution energies of dopants on various sites, with various charge compensation models [18–21]. For Zn, Araujo *et al.* [18] found that the self-compensating model with 75% of Zn on a Li site and 25% of Zn on a Nb site has the lowest solution energy for bound defects, which is inconsistent with the EXAFS analyzes. However, these calculations were carried out for $T = 0$ and 293 K, and assumed the dopant and associated charge compensator ions were in thermal equilibrium in stoichiometric material. Xu *et al.* [20] using DFT calculations note that the site occupation will depend on the chemical potential, and when it is close to that for congruent material, both 2+ and 3+ defects are on the Li site, with Li vacancies (V_{Li}) for charge compensation—but they only considered a few dopants and did not consider Zn. In addition, if the chemical potential is close to that for stoichiometric material it is more complex—for Fe^{2+}, Fe substitutes on Li

*bridges@ucsc.edu

(slightly lower energy) while Mg^{2+} has a lower energy for self-compensation with Mg on both Li and Nb sites (75% and 25%, respectively) as found by Araujo *et al.*

For 3+ defects such as In^{3+} or Er^{3+}, and 4+ defects such as Hf^{4+}, solution energies have also been calculated for bound defects. Xu *et al.* [20] considered three defect clusters [schemes (i), (ii), and (iii) in the next section] and found that for (Fe^{3+}, Nd^{3+}, and Er^{3+}) in stoichiometric material, the self-compensation configuration with 50% on each site has the lowest energy; while for congruent material, substitution is on the Li site. Araujo *et al.* [18,19,22] have also considered a number of substitution schemes for such defects which are summarized below.

The EXAFS experiments reported here investigate the substitution sites for univalent 3+ and 4+ dopants in both cLNO and sLNO. Codoped samples and samples with multivalent dopants are excluded at this point because the local structure could be more complex. In and Hf ions are both considered to be optical damage resistant (ODR) ions. Rare earth ions such as Er are incorporated into LNO to serve as laser activators [23] and for optical hole burning applications [24]. EPR experiments indicate that in codoped samples (Er plus a threshold concentration of Mg or Zn), a broad, strong new resonance is observed that is attributed to Er on a Nb site [25]. This suggests that in stoichiometric samples Er dopants may also have a significant fraction of Er_{Nb}; recently a low concentration (few percent) of Er_{Nb} in sLNO has been observed using OH^- vibrational spectroscopy [26]. In general it is assumed that when the concentration of Nb_{Li} antisite defects is low, as is the case for stoichiometric crystals, it promotes the occupation of the Nb site, and we have included two stoichiometric samples to see if significant occupation of the Nb site occurs.

A. Substitution models for In and Er

Araujo *et al.* [18,19] considered four different schemes for In^{3+} and Er^{3+} substitution in sLNO; the three schemes with the lowest energies are listed below using Kröger-Vink notation [27]; here M = In or Er. The numbering of Araujo *et al.* [18,19] and Xu *et al.* [20] are the same for schemes (i)–(iii)). [Scheme (iv) has different compensating defects compared to (iii), but has a higher energy.] For calculations at 0 K, the solution energies for In are nearly identical for schemes (ii) and (iii) but scheme (ii) is lowest for calculations at 293 K. For In, scheme (i) has higher energies at 0 and 293 K, but has the largest decrease with increasing temperature. For Er, scheme (ii) has the lowest energy at 0 K, but scheme (iii) is lower at 293 K. All dopants are on the Li site for scheme (i) while 50% of dopants are on the Li site for scheme (ii); in scheme (iii) all the dopants are on the Nb site.

(i) $M_{Li}^{\bullet\bullet} + 2V_{Li}'$,

(ii) $M_{Li}^{\bullet\bullet} + M_{Nb}''$,

(iii) $2M_{Nb}'' + Nb_{Li}^{\bullet\bullet\bullet\bullet}$.

B. Substitution models for Hf

Recently Araujo *et al.* [22] have also calculated the solution energies for the Hf^{4+} defect in sLNO. Here they considered seven different schemes, but schemes (iii) to (vii) have all Hf only on a Nb site, with different charge compensation defects. Scheme (i), which is the only defect model with all Hf on a Li site, has a very large defect solution energy; the schemes with the three lowest energies are tabulated below. At both 0 and 293 K, scheme (vi) has the lowest energies, while scheme (ii) is second lowest—however, the energies for these three models differ by less than a factor of 2. For the self-compensating scheme (ii), 25% of Hf are on the Li site; 75% on Nb site.

(ii) $Hf_{Li}^{\bullet\bullet\bullet} + 3Hf_{Nb}'$,

(iii) $4Hf_{Nb}' + Nb_{Li}^{\bullet\bullet\bullet\bullet}$,

(vi) $3Hf_{Nb}' + Nb_{Li}^{\bullet\bullet\bullet\bullet} + V_{Li}'$.

TABLE I. Ionic radii tabulated by Shannon [28] for different dopants and host cations with sixfold coordination. The O^{2-} ionic radius corresponds to an oxygen in fourfold coordination with its neighbors. The much larger radius of Er^{3+} compared to other ions results in the larger positive shifts in bond length for Er-O bonds.

Atom	Valence	Radius (Å)
Li	1+	0.76
Nb	5+	0.64
Zn	2+	0.74
In	3+	0.80
Er	3+	0.89
Hf	4+	0.71
O	2−	1.38

C. Ionic radii

An important aspect to consider in discussing the occupation sites for the dopants is the ionic radius of the dopant and how it compares to the host cations. We list a few relevant ionic radii in Table I for sixfold coordinations. These radii together with that of O^{2-} can be used to estimate the average M-O distances for the first O shell about the dopant. Note that the average Li-O and Nb-O distances in the first O shell in the host material agree well with this empirical approach. (For example, bond lengths for Li-O are 2.06 and 2.26 Å; average = 2.16 Å. Sum of ionic radii for Li^+ and O^{2-} is 2.14 Å.) Using the ionic radii and ignoring corrections for octahedral distortions [28], we can roughly predict the expected M-O distances for the first shell about the dopant: In 2.18 Å, Er 2.27 Å, and Hf 2.09 Å. All dopants have larger ionic radii than Nb, with Hf the closest in size (only 0.07 Å larger). Thus from ionic radii considerations alone, occupation of the Nb site appears less likely for In and Er. Substituting a larger ion for a smaller one will introduce significant distortions.

D. Local structure about the Li and Nb sites

The local environments about the Li and Nb sites are shown in Fig. 1, based on the known crystal structure for $LiNbO_3$ (space group $R3c$). For the Li site in the undistorted crystal there are four Nb neighbors at ∼3.06 Å, and additional Nb neighbors at ∼3.36 and 3.88 Å. Around the Nb site, there are

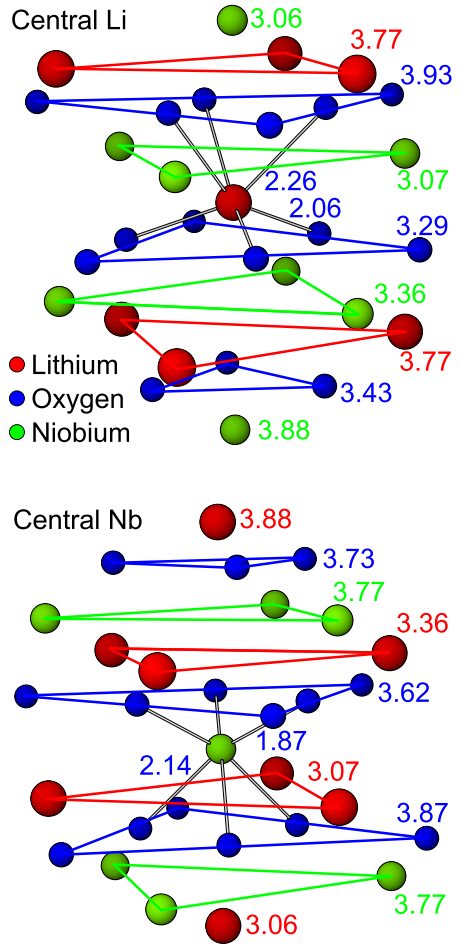

FIG. 1. The environment about the Li (top) and Nb (bottom) sites in $LiNbO_3$. Bonds are shown for the nearest O atoms and the pair distances for the first few shells are indicated for each site.

Li neighbors at ∼3.06, 3.36, and 3.88 Å, with the first Nb neighbor at 3.77 Å; because Li is such a low Z element the M-Li contributions are tiny compared to M-Nb peaks. As a result there is a very large M-Nb peak in the EXAFS r-space data near 2.9 Å for substitution on the Li site but a much lower amplitude over the 2–3 Å range for defects on an Nb site; the largest peak for the Nb substitution site occurs near 3.6 Å. This provides a guide for setting up fits of the data. (See for example, Figs. 4 and 5 in Ref. [16].)

II. EXPERIMENTAL DETAILS

In-doped $LiNbO_3$ crystals were purchased from Impex High Tech, Germany, with nominal (melt) In concentrations of 1 and 4 mol %. The actual In concentrations, measured from the ratio of the In and Nb edge step heights [17,29], are 0.7 and 2.8 mol %. The Er- and Hf-doped crystals were grown at the Wigner Research Centre in Budapest. A cLNO crystal doped with 6 mol % Er was grown from melt by the Czochralski method. The other Er- and the Hf-doped sLNO crystal were grown from solution using the high temperature top seeded solution growth method [30]. For the Er-doped $LiNbO_3$ crystals the defect concentration is

TABLE II. Summary of dopants studied and type of host crystal (sLNO or cLNO) with measured concentrations given in mol %.

	cLNO	sLNO
In	0.7	
In	2.8	
Er	2.3	
Er		0.55
Hf		0.57

0.55 ± 0.11 mol % in sLNO [26] and 2.3 ± 0.15 mol % in cLNO; the latter was measured using the inductively coupled plasma optical emission spectrometry (ICP-OES) method. Finally, the Hf concentration in sLNO is 0.57 ± 0.02 mol %, using the inductively coupled plasma mass spectrometry (ICP-MS) method. For each material, powdered samples for EXAFS measurements were prepared as described in Ref. [16]; a summary of samples and concentrations is given in Table II.

EXAFS data were collected at the In K edge in fluorescence mode, for 0.7 and 2.8 mol % In-doped congruent $LiNbO_3$, using beamline 4-1 at the Stanford Synchrotron Radiation Lightsource (SSRL). Data were collected at 10 and 300 K in an Oxford helium cryostat, using a 220 monochromator; a slit size of 0.3 mm provided an energy resolution of 4.0 eV. Harmonic content was reduced by detuning the monochromator 50% at 28 100 eV.

Data for the Er-doped samples were collected at the Er L_{III} edge in fluorescence mode on beamline 4-1 at 10 K; a 220 monochromator was used with a vertical slit size of 0.6 mm, giving an energy resolution of 0.8 eV. Harmonic content was reduced by detuning the monochromator 50% at 8600 eV. Finally 10 K data at the Hf L_{III} edge for sLNO:Hf were collected in fluorescence mode using the focused beamline 9-3, with vertical slit size of 0.2 mm.

The EXAFS data were reduced and the k-space functions obtained at each edge using the program RSXAP [31], which uses standard techniques to remove the backgrounds, below and above the edge. Examples of the k-space data (k^2 weighting) for each edge are shown in Fig. 2.

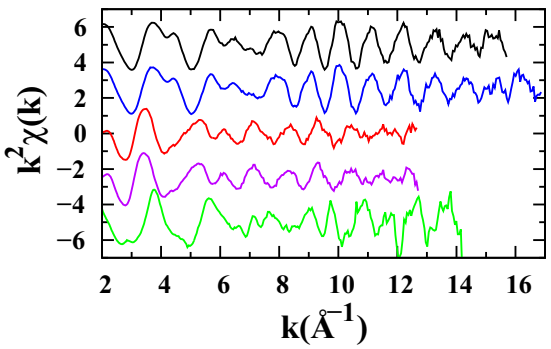

FIG. 2. $k^2\chi(k)$ vs k from top to bottom: at the In K edge, black cLNO, 0.7 mol % In, blue 2.8 mol % In; at the Er L_{III} edge, red sLNO, 0.55 mol % Er, purple cLNO, 2.3 mol % Er; and at the Hf L_{III} edge, green sLNO, 0.57 mol % Hf. The plots are displaced vertically for clarity.

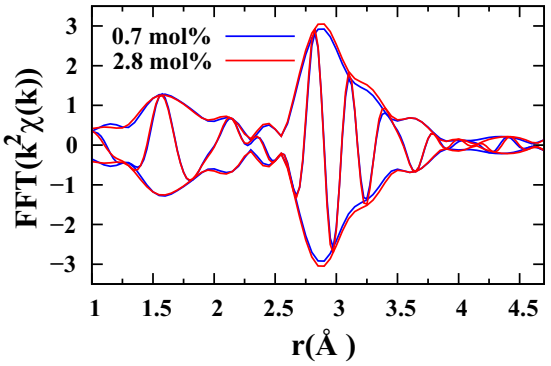

FIG. 3. Comparison of the r-space data (FT $k^2\chi$) for 0.7 and 2.8 mol % In-doped cLNO at 10 K. The FT range is 4.1–14.7 Å^{-1}. The differences between the two traces are very small, with the largest deviations in the 2.75–3.25 Å range. In this and subsequent r-space plots the fast oscillation is the real part R of the FT while the envelop function is $\pm\sqrt{R^2+I^2}$ where I is the imaginary part of the FT.

III. EXAFS DATA AND ANALYSIS

A. Data

The $k^2\chi(k)$ data were fast Fourier transformed (FT) into r space and are plotted in Figs. 3 and 4. The 0.7 and 2.8 mol % In r-space data (In K edge) are compared at 10 K in Fig. 3 using an FT range of 4.1–14.7 Å^{-1}; the two traces are nearly identical indicating no significant change between these concentrations. Similar data at 300 K (not plotted) show similar functions, but with a decreased amplitude from thermal broadening. The very large amplitude peak near 2.9 Å in the EXAFS plot, is a signature of substitution on a Li site, but the peak position on the EXAFS plot is shifted to lower r by a well known phase shift; this is typically 0.2 Å for heavy backscattering atoms but larger for O atoms ∼0.4 Å.

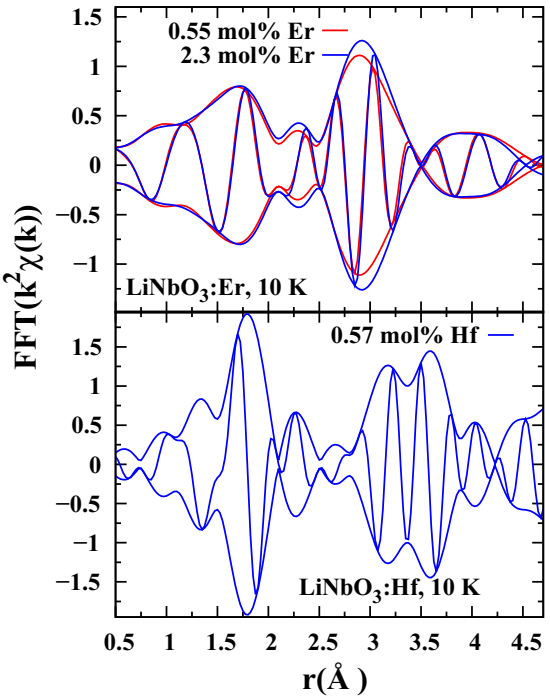

FIG. 4. Top: Comparison of r-space data at 10 K for 0.55 mol % Er in sLNO (red) and 2.3 mol % Er in cLNO (blue). The largest change is at the Er-Nb peak near 2.9 Å which is smaller in the sLNO sample, suggesting possibly less Er on the Li site for sLNO. The FT range is 4.1–11.5 Å^{-1}. Bottom: r-space data at 10 K for 0.57 mol % Hf in sLNO (blue). Note the smaller amplitude near 2.9 Å, and the larger peak near 3.6 Å compared to the Er (or In) data, indicating some Hf is on an Nb site. FT range is 3.8–12.7 Å^{-1}.

Similar r-space data for the Er substituted sample (Er $L_{\rm III}$) are shown in the top panel of Fig. 4 for a shorter FT range 4.1–11.5 Å^{-1}. The traces for the stoichiometric material (0.55 mol % Er) and congruent material (2.3 mol % Er) are quite similar and overlap well for the short Er-O peaks (near 1.7 Å on plot) and also near 4 Å. However, there is a noticeable difference near 2.9 Å, where the largest peak is observed; it is attributed to an Er-Nb peak with Er on a Li site. Whether the number of Er-Nb bonds changes between samples (from a small change in defect site occupations) or the peak is broadened from disorder, requires detailed fits.

The r-space plot for Hf substituted sLNO is shown in the lower panel of Fig. 4 and is quite different from either the In or Er $L_{\rm III}$ edge EXAFS data; FT range 3.8–12.7 Å^{-1}. The most striking differences are the larger amplitude near 3.6 Å (actual distance ∼3.8 Å), where an Hf-Nb peak should occur for substitution on a Nb site, and the low amplitude near 2.9 Å, where the Hf-Nb peak would occur for substitution on an undistorted Li site. Surprisingly the Hf-O peak near 1.75 Å, is also larger for the Hf data. The significant difference in amplitude over the 3 to 4 Å range suggests that a significant fraction of the Hf occupies an Nb site.

B. Fits of data

To fit the EXAFS data we follow the same approach as used in the earlier studies of Zn-doped sLNO and cLNO [16,17]. The data are fit in r space to a sum of peaks corresponding to different shells of neighbors about the dopant. Theoretical EXAFS functions for each peak were calculated using FEFF7 [32]. For the In and Er dopants, the large peak near 2.9 Å corresponds to a M-Nb peak, when a large fraction of metal (M) dopants is on the Li site; for Hf the lack of a strong peak near 2.9 Å and the large peak near 3.6 Å indicates some substitution occurs on the Nb site. For each type of site there are also some weak M-Li pairs, and at longer distances some weak multiscattering peaks, but most of these are negligible. The fits at each edge and the significant results are discussed below; further details about the fits are provided in the Supplemental Material [33].

For the In-doped samples the same model fits the data sets for both 0.7 and 2.8 mol % In samples. There are two short In-O bonds, with longer In-O peaks near 3.3 and 3.9 Å. Note that for an undistorted Li site there are two intermediate Li-O distances at 3.29 and 3.43 Å, but these could not be resolved in the Zn data (two peaks moved together) and were fit with an average peak near 3.29 Å [17]; a similar result is found here. The expected In-Nb pair distances are near 3.06, 3.36, and 3.87 Å. Overall, the In-O pairs have slightly

TABLE III. Fit parameters for fits of the In data. The In-O3 peak near 3.3 Å is a sum of two peaks at nominally 3.29 and 3.43 Å in pure $LiNbO_3$. (Only the average 3.36 Å is listed below, under diffraction. The In-In peak assumes that In-In pairs form in Li sites 3.77 Å apart.)

	Diff.	In 0.7 mol %, cLNO		In 2.8 mol %, cLNO	
Atom pair	r (Å)	r (Å)	σ^2 (Å^2)	r (Å)	σ^2 (Å^2)
In-O1	2.06	2.08	0.0020	2.07	0.0019
In-O2	2.26	2.22	0.0043	2.22	0.0039
In-Nb1	3.06	3.21	0.0025	3.21	0.0024
In-O3	3.36	3.31	0.0056	3.30	0.0046
In-Nb2	3.36	3.47	0.0032	3.47	0.0032
In-In	3.77	3.85	0.0020	3.86	0.0020

shorter distances on average while the In-Nb pair distances are slightly increased (see Table III), as found earlier for the Zn substituted samples. This model fits very well up to 3.5 Å, but above 3.5 Å, the fit amplitude is too low. Various models were tested, including increasing the Nb-site occupation of the In dopant. This approach did not work well (see the Supplemental Material [33]), and we then considered the possibility of pairs of In atoms on closest Li sites, ∼3.77 Å apart. This would add an In-In peak with one neighbor at a distance near 3.8 Å. Surprisingly, this gave a better fit than adding an extra (one neighbor) In-Nb peak at roughly the same distance. Although strongly suggestive that In-In pairs do form it is not conclusive as the amplitude near 3.6 Å is small. In the final fits 16 parameters were varied with five degrees of freedom remaining [34]. Plots of the fits for 0.7 mol % In at both 10 and 300 K are shown in Fig. 5 and the results at 10 K are summarized in Table III; the fraction of In on an Nb site is <5%.

For the Er substituted samples, the peak near 2.9 Å is smaller compared to the In data, suggesting that some of the Er might be on an Nb site. This complicates the analysis because then there are distinct peaks for each site, and the FT range is limited compared to In, see Fig. 2. Again we use two peaks for the first O shell and used the same model for Er on a Li site as used for In. The region from 3.8–4.5 Å has a sum of many Er-O peaks and is roughly modeled by a large amplitude Er-O peak; this served well and did not introduce an excess of parameters. Initially we found that a fit including only Li site occupation results in a reasonable fit, but wanted to investigate if the fit would improve if some of the Er were on a Nb site. An Er-Nb peak was added at 3.77 Å, plus a Nb site Er-O peak at 3.62 Å; in addition the FT range was increased by shifting the start of the FT range to lower $k - k_{\min} \sim 3.5$ Å^{-1}. However this can include structure from XANES—see the Supplemental Material [33]. We also employed a parameter f_1 as the fraction on a Li site, with $(1 - f_1)$ on the Nb site.

The overall result is that with a k window that excludes a significant XANES contribution, we find that Er data are fit well with a lithium-site only model (some uncertainty between scans), with large positive shifts in pair distances due to the large ionic radius of Er. Since the fits including Nb site peaks were of similar quality (but with more parameters) to those for the Li site alone, we estimate that the Nb site occupation is ∼5%−10%, with a maximum upper bound of ∼14%; this higher uncertainty of Nb site occupation compared to In is in part a result of the shorter FT range. We also tested whether the inclusion of an Er-Er peak (that would arise from clustering on two Li sites), would improve the fits. Based on the Hamilton F-test [35] this peak was not significant and was not included in later fits. In the final fits using k^2 weighting, a fit range of 1.1–4.6 Å, and an FT range 4.1–11.5 Å^{-1}, 16 parameters were varied and two degrees of freedom remain. These fits for data at 10 K for the sLNO and cLNO samples are shown in Fig. 6 and the parameters are tabulated in Table IV. Additional details are provided in the Supplemental Material [33].

The Hf r-space data, plotted in Fig. 4, show an interesting double-peak feature around 3.5 Å that is quite different from the corresponding data for other dopants, and suggests a

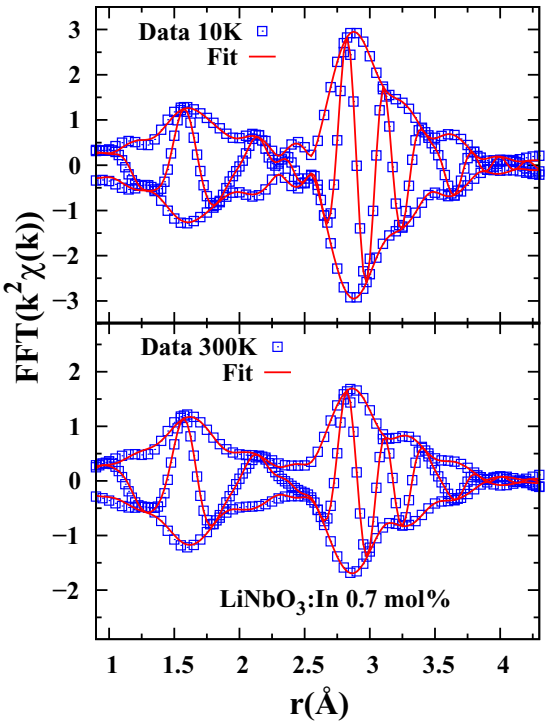

FIG. 5. Fits of the r-space data (FT $k^2\chi$) for 0.7 mol % In-doped $LiNbO_3$ at 10 and 300 K (data blue squares; fit red lines); see text for model. The amplitude at 300 K is significantly reduced from thermal vibrations for the In-Nb peaks above 2.5 Å. The FT range is 4.1–14.7 Å^{-1}, while the fit range is 1.2–3.9 Å; $S_0^2 = 1.0$.

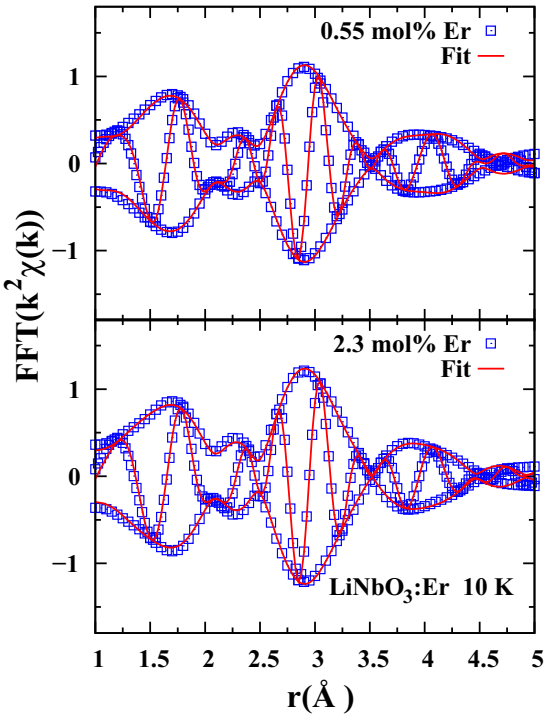

FIG. 6. Fits of the 0.55 mol % Er (sLNO) and 2.3 mol % Er (cLNO) at 10 K (data blue squares; fit red line). A good fit is achieved up to ∼4.5 Å; see text for model and Table IV for main parameters. The FT range is 4.1−11.5 $Å^{-1}$ and fit range is 1.1–4.6 Å.

mixture of Li and Nb site substitution. A similar model to that used for Er is applied for Hf—but starting with the fractions on the two sites more comparable. For the restricted range, 2.6–4.0 Å, on the EXAFS plot; the dominant Hf-Nb peaks are: two peaks for a Li site substitution [four neighbors at 3.07 Å and three neighbors at 3.36 Å (actual distances)], and one peak for a Nb site substitution (six neighbors at 3.77 Å). Although there are (weaker) Hf-O and multiscattering peaks in this range, an approximate fit can be achieved using only these peaks. The amplitudes of the peaks are constrained using the number of neighbors in each shell about Li and Nb, plus the fraction f_2 (varying from 0 to 1), which represents the fraction of Hf on the Nb site, i.e., $A_i = N_i f_2$ when Hf substitutes on Nb (N_i is the number of neighbors in the ith shell about Nb), and $A_i = N_i(1 - f_2)$ for Hf on a Li site. For this restricted fit $f_2 \sim 0.55$ and the position of the Hf-Nb peak for a Nb site substitution, shifted very little from that for the host distance. In contrast the Hf-Nb distances for the Li site substitutions increased considerably. See the Supplemental Material [33] for further details. In a full fit the positions of the Nb neighbors do not shift much from this restricted fit and the parameters are tabulated in Table V. An example of the full fit which includes some longer multiscattering (MS) peaks is shown in Fig. 7. From many different fits with O and MS peaks included, the fraction f_2 is about $50 \pm 10\%$; thus our result is that half of the Hf occupies the Li site and half occupies the Nb site.

IV. DISCUSSION

The important results from the detailed fits of the EXAFS data are: (1) In^{3+} substitutes primarily on the Li site and the results are nearly identical for two concentrations of cLNO (0.7 and 2.8 mol %); this result is very similar to that for the Zn^{2+} defect [17]. (2) Similarly for Er^{3+}, almost all Er is on the Li site (∼90%); the fraction on the Nb site for the sLNO sample (0.55 mol % Er) is consistently slightly larger (about 5%) than for cLNO sample (2.3 mol % Er) when the f_1 parameter is allowed to vary in the fit. (3) The Hf^{4+} ion (0.57 mol % in sLNO) substitutes roughly half on a Li site and half on a Nb site. This is the first clear evidence for significant dopant occupation of the Nb site for any dopant we have studied, and to our knowledge no other EXAFS study has observed a large dopant fraction on Nb. (4) There is a significant difference in the magnitude and extent of local distortions about different types of dopant at comparable concentrations. The extent of disorder is very important as it leads to broadened optical and EPR linewidths and also changes the photoconductivity. These results are inconsistent with a purely self-compensating scheme for each dopant [see scheme (ii) in Sec. I A] and therefore require one and usually more nearby charge compensating defects; the most likely are Li vacancies, V_{Li}, but some Nb_{Li} may still exist, particularly for Hf. Since there are many nearby Li sites within a 6 Å radius about a Li site, a large number of possible distributions exist. What distributions form at high temperatures and are they in thermal equilibrium or metastable in nature?

The extent of local disorder deserved further discussion as it may broaden optical linewidths in some applications. First we compare the average M-O distances in the first oxygen shell with the predictions from ionic radii (see Table I). The measured average In-O bond length is 2.15 Å, only 0.03 Å smaller than predicted from ionic radii; similarly, the Er-O

TABLE IV. Table of significant fit parameters. Due to the relatively large ionic radius of Er, all significant peaks have a positive shift in bond length. Note the Er-O3 peak is a sum of peaks at 3.29 and 3.43 Å in undistorted crystal; average distance 3.36 Å. The difference between the stoichiometric and congruent sample is negligible.

	Diff.	Er 0.55 mol %, sLNO		Er 2.3 mol %, cLNO	
Atom pair	r (Å)	r (Å)	σ^2 ($Å^2$)	r (Å)	σ^2 ($Å^2$)
Er-O1	2.06	2.15	0.0030	2.15	0.0025
Er-O2	2.26	2.33	0.0056	2.34	0.0041
Er-Nb1	3.06	3.28	0.0035	3.29	0.0021
Er-O3	3.36	3.59	0.0052	3.56	0.0061
Er-Nb2	3.36	3.39	0.0057	3.43	0.0050

TABLE V. Fit parameters for the Hf L_{III} edge data. The subscript on the pair indicates the substitution site, except for Hf-O2; this peak is the sum of three peaks at distances 2.06 and 2.26 Å from the Li site and 2.14 Å from the Nb site; average distance 2.15 Å (for 50% occupation of each site). The average Li site Hf-O3 distance in the undistorted lattice is 3.36 Å, the average of 3.29 and 3.43 Å. Similarly the Nb site average Hf-O4 distance is 3.673 Å, the average of 3.620 and 3.73 Å. For this particular fit the fraction of Hf on an Nb site was 53%; however because of interference, the fit is sensitive to the initial parameters—in particular, the values for σ^2 and the substitution site fraction are correlated. From many different fits the occupation is 50 ± 10% on each site. The errors for σ^2 are also large ∼10%.

	Diff.	Hf 0.57 mol %, sLNO	
Atom pair	r (Å)	r (Å)	σ^2 (Å^2)
$(Hf\text{-}O1)_{Nb}$	1.87	1.89(1)	0.0028
Hf-O2	2.15	2.08(1)	0.0013
$(Hf\text{-}Nb)_{Li}$	3.07	3.13(1)	0.0043
$(Hf\text{-}O3)_{Li}$	3.36	3.09(2)	0.0021
$(Hf\text{-}Nb2)_{Li}$	3.36	3.54(2)	0.0013
$(Hf\text{-}Nb3)_{Nb}$	3.77	3.75(2)	0.0015
$(Hf\text{-}O4)_{Nb}$	3.67	3.72(4)	0.021

average bond length is 2.24 Å, again about 0.03 Å shorter than predicted from ionic radii. For Hf the difference is larger, but here Hf has a large occupation on both the Li and Nb sites. Including occupation fractions, the average weighted Hf-O distance is 2.03 Å, 0.06 Å shorter than that predicted from ionic radii. However the trend for the M-O bond lengths clearly agrees well with the ionic radii of the dopant cations.

Less well understood is that the ionic size and dopant valence also play a role in the displacements of the first few shells of Nb further neighbors about the Li site and hence

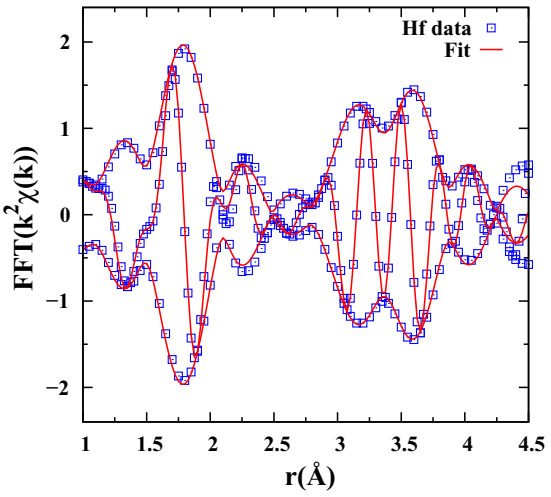

FIG. 7. Fits of the 0.57 mol % Hf (sLNO) at 10 K (data blue squares; fit red line). A good fit is achieved up to 4.5 Å; see text for model and Table IV for main parameters. The FT range is 3.8–12.7 Å^{-1} with a Gaussian rounding of the FT window by 0.2 Å^{-1}; the fit range is 1.0–4.2 Å.

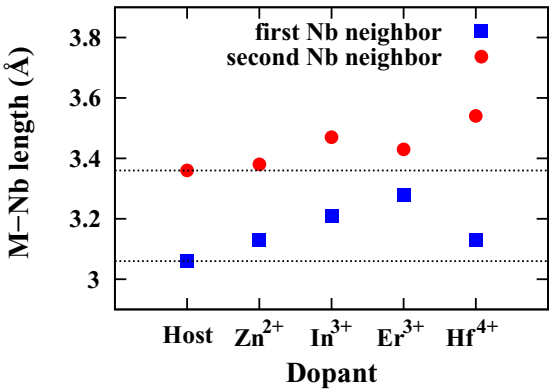

FIG. 8. M-Nb distances for the first two Nb neighbors about the Li site vs type of dopant on the Li site. The dotted horizontal lines are the Li-Nb distances at 3.06 and 3.36 Å for the undistorted lattice. The M-Nb pair distances increase with valence (and also the dopant ionic radius) except for the Hf dopant.

the extent of disorder introduced into the lattice by different dopants.

The first two M-Nb pair distances are plotted in Fig. 8 vs type of dopant. Both distances increase as the dopant ionic radius increases from Zn to Er; however the shift is larger for the closest Nb atoms. Since in Fig. 1 top the 3.06 Å Nb atoms are above the central Li while the 3.36 Å Nb atoms are below, it might be inferred that a difference in shifts of these two pair distances might indicate that the dopant atom is also slightly displaced from the Li site in LNO along the c axis as proposed by Baumann *et al.* [36]. However, one cannot easily distinguish between a displacement of the central atom and displacements of neighboring shells of atoms. We return to this aspect later when discussing some x-ray standing wave measurements. Also it is very unlikely that any dopants are on some other interstitial site; for a random site with low order, the peaks in the EXAFS would be strongly suppressed by the disorder, which is not observed. For the interstitial sites along the c axis, the Nb neighbors would be closer than for the Li site—with one Nb neighbor very close at 1.94 Å. Such close Nb neighbors would be inconsistent with the data.

For Hf the situation is more complex; first note (Table V) that for the fraction of Hf on an Nb site, the changes in pair distances compared to the host, are very small $\leqslant$0.02 Å. Much larger changes are observed for the fraction of Hf on a Li site; however, the displacement of the closest Nb neighbor is smaller (∼0.06 Å) than for the second Nb neighbor (∼0.18 Å). For the closest Nb neighbor, this may be a competition between the small ionic radius for Hf (which would tend to shorten the distance) and the increased Coulomb repulsion when Hf^{4+} replaces Li^+ (which would lengthen it).

Three other EXAFS studies have investigated the local structure about several dopants in LNO, including the Er and Hf defects—but only collected data at room temperature [37–39]. The first EXAFS studies were done before the FEFF codes [40,41] that enabled detailed fits over several shells of neighbors, were readily available. In contrast, in our study, with good data out to much higher values of k, a detailed investigation of the second and third Nb neighbor environments

is possible; this region in real space is where the strongest fingerprint for Li or Nb site occupation resides, and our result contradicts some studies done with older analysis packages.

Prieto *et al.* [37,38] indicated that they used the old theoretical phase and amplitude functions from McKale *et al.* [42] and reported that Hf substitutes on the Li site, but the room temperature data are very noisy. They find a broadened Hf-O peak (2.07 Å) for cLNO close to the average Hf-O distance we observe (2.03 Å), but for Hf-Nb, the dominant contribution they report is six Nb neighbors at 3.30 Å, with little evidence for a peak near 3.77 Å that would be indicative of some Nb substitution. A coordination number of six neighbors is not consistent with the Li site environment, unless for their shorter k range, several Hf-Nb peaks could not be resolved, and are treated as a single peak. Note that their room temperature data do not show the double peak structure we observe between 3 and 4 Å for $T = 10$ K; see Fig. 7. In a later study [39] they use an early version of FEFF (FEFF3) [43] to calculate the EXAFS functions for neighbors about Hf, but used the same data [37]; the fit results for $LiNbO_3$:Hf are similar with small shifts in the neighbor positions.

Zaldo and Prieto [38] also report that Er substitutes on the Li site for cLNO, for dopant concentrations within the range 0.5 to 1 mol %. Unfortunately, no data are shown but the fit results are tabulated. For Er, they report a very short Er-O distance (2.0 Å), even shorter than the average Li-O distance in pure LNO (2.16 Å), although the ionic radius of Er^{3+} is significantly larger than Li^+. The second Er-Nb peak is surprisingly long. Also the values of σ^2 they report are very large (roughly a factor of 10 larger than reported here for 10 K) indicating that the EXAFS are highly damped, and the local structure very disordered.

For In^{3+} and Er^{3+} substitutions, other types of probes generally agree with the primarily Li site substitution reported here, although the fraction of dopant on the Nb site is usually not provided. Kong *et al.* [44] propose that In^{3+} occupies Li sites for concentrations up to about 3 mol % based on OH^- IR spectroscopy, but for higher concentrations—near 5 mol %—some In moves onto the Nb site. Similarly Hauer *et al.* using perturbed angular correlations (PAC) [45], find In on the Li site.

Rebouta *et al.* [46] have carried out PIXE/channeling experiments on Er-doped cLNO and find a significant fraction of the Er is on a Li site. but suggest that at least 50% of the Er is not on either the Li or Nb site, but instead on some interstitial site. However, interstitial sites have much closer Nb neighbors than do the Li and Nb lattice sites, and because of the large backscattering from heavy Nb neighbors, this would provide a strong signature—a short M-Nb distance, which is not observed. In addition, more disorder is expected around an interstitial site. Part of the difference with their work might be attributed to a higher Er concentration (about 4 mol %) in their cLNO sample.

Gog *et al.* [47] and Baumann *et al.* [36] have used x-ray standing waves to investigate Er diffused into a cLNO crystal, in a region close to the crystal surface. They report substitution near the Li site but suggest that Er is displaced from the usual Li position by 0.46 Å along the c axis with no distortion of the host lattice; on Fig. 1 top this would be a −0.46 Å downward displacement of Er_{Li}. Although the local environment about Er is distorted the largest distortions we observe are <0.23 Å; in addition all the Er-Nb pair distances increase which is not consistent with a simple downward displacement of Er, i.e., a large displacement of Er along the c axis would make some Er-Nb pair distances longer and others shorter. Note also that for the nearest O atoms above and below Er_{Li}, the Er_{Li}-O distances both increase by comparable amounts (attributed to the much larger ionic radius for Er) which would be inconsistent with the above model with no distortion of the host lattice; if Er_{Li} is displaced, the first O shell follows it.

An important aspect for all compensated defects is that there must be many, slightly different local site distributions, consistent with the discussion above. This had been deduced explicitly from high resolution optical spectroscopy for the Er^{3+} ions, where many very sharp lines have been observed [48,49], and from EPR spectra where many lines are also observed [50]. In both cases, these complex spectra have been attributed to slightly different arrangements of the nearby charge compensating Li vacancies, but also from pairs or other clusters [48]. The EPR results have been interpreted in terms of a statistical distribution of V_{Li} on nearby Li sites [50]. So far however the specific local distributions of other defects have not yet been determined. Also note that the relatively small size of σ^2 for all atom pairs in the EXAFS analysis (Table IV) means that the environments about each dopant are very nearly the same, i.e., well ordered; any variations in the arrangements of V_{Li} compensators do not provide much variation in the local disorder, even when it is distorted.

For Hf, Hammoum *et al.* [51] used Raman spectroscopy to study a doped cLNO crystal. They argue that at low concentrations, Hf replaces the Nb_{Li} antisite defects, while at high concentrations above ∼4.5 mol %, Nb sites also become occupied. Their results are qualitative as no occupation fractions are given. It is likely that their high concentration samples are more comparable to the sLNO samples studied here, as then all the Nb_{Li} antisites are likely filled. Kovács *et al.* [52] also find that above a threshold concentration a small fraction of Hf occupies the Nb site.

Marques *et al.* [53] use a combination of Rutherford backscattering and channeling (RBS/C) and PAC to investigate the substitution site(s) in a near-stoichiometric crystal with 1 mol % Hf, and a cLNO crystal with ∼6 mol % Hf. They also found Hf substitutes on both sites, with more Hf on the Nb site for the near stoichiometric sample but more on the Li site for the cLNO sample. Qualitatively, the site fractions are similar to our results; however they report that there are two different Hf_{Nb} sites with one of them displaced by 0.1 Å. This would introduce considerable disorder about the Hf_{Nb} sites. A striking aspect of the EXAFS results is that for the fraction of Hf on a Nb site, distortions of the first O and Nb shells are very small (∼0.02 Å) and the disorder (σ^2) is also small.

These EXAFS results do not agree as well with some calculations using pair potentials [18,19,22]—see the Introduction for a brief summary of such results. For In, the EXAFS are consistent with scheme (i), in which all In^{3+} are on a Li site in cLNO; this also agrees with the DFT calculations for 3+

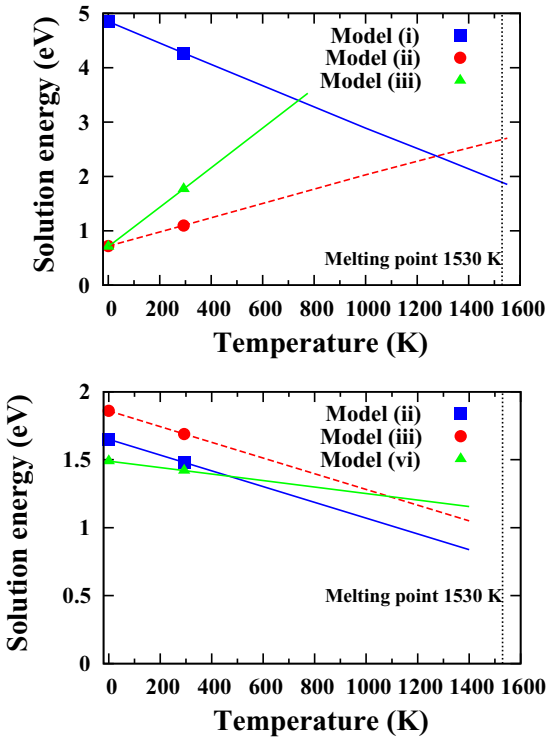

FIG. 9. Top: Plot of the solution energies of In dopants for models (i), (ii), and (iii) of Ref. [19] as a function of T to show extrapolations to higher T. These extrapolations suggest that the lowest energy model may change when the defect is frozen in at high temperatures, thus motivating defect calculations at much higher temperatures. Bottom: Similar extrapolations for the three lowest energies for Hf dopants [22]. Although scheme (vi) is lowest below room temperature, scheme (ii) is lower at high T.

ions [20], assuming that the chemical potential is close to that for cLNO. Using pair potentials however, the lowest solution energy scheme is the self-compensating model (ii) [19]; if these theoretical results [19] at 0 and 293 K are extrapolated to high temperatures, scheme (i), with all In on a Li site, eventually becomes the lowest solution energy, see Fig. 9 top.

For Er, the EXAFS results suggest a similar scheme to In [scheme (i)—90% on Li]. The major difference between trivalent In and Er is the ionic radius, where Er is considerably larger. In the DFT calculations [20] Er is on a Li site [scheme (i)] for a chemical potential close to cLNO while it is self-compensated [scheme (ii)] if the chemical potential is close to that for stoichiometric material, but the disparity in ionic radius between Er and Nb implies a bias for scheme (i). We find no significant difference in local structure between Er-doped cLNO and sLNO. Even though Er and In share a similar doping scheme the local environment around the impurity differs, as is evident in the larger M-Nb bond-length shifts in LNO:Er and in the increased amount of disorder observed in the k-space data in Fig. 2; we believe this is due to the difference in ionic radii. Subtle differences in the defect complex (impurity atom plus surrounding charge compensating defects) are significant when trying to carefully control optoelectronic response in engineered devices.

For a low concentration Hf dopant in sLNO, the EXAFS results indicate an approximate 50–50 occupation of the Li and Nb sites. For this dopant, calculations [22] using pair potentials at 293 K indicate that scheme (vi) (all Hf on Nb) has the lowest solution energy, but only slightly lower than scheme (ii) (25 % Hf on Li) as shown in Fig. 9 bottom. However, to have the 50–50 occupation on the two sites means there must also be a significant contribution from scheme (i), with all Hf on a Li site. Why the fraction of Hf on a Li site must be large is not clear as scheme (i) has a large solution energy.

These results raise several issues about the assumptions on which the calculations are based. First the samples are grown at very high temperatures (melting point about 1530 K) and as solidification takes place, are the dopant atoms uniformly distributed? At these high temperatures is there a different preference for the substitution site? Second as the crystal cools slowly, are the locations of the heavy atoms (including the dopants), quenched in, or is diffusion sufficient to allow for equilibrium to be achieved? Alternatively, are the room temperature samples in a metastable state? Light Li ions diffuse easily [54] at 250 °C and consequently V_{Li} can easily provide charge compensation for a wide range of temperatures. Since there are many nearby locations for V_{Li} charge compensators, a large number of slightly different dopant-compensator complexes are possible as observed for Er^{3+} [48,50], and likely exist for all other dopants. In contrast, heavy atoms diffuse much more slowly—for example even the relatively light Ti atom takes 50 h at ~1370 K to diffuse a few micron [12]. Much heavier atoms such as Nb may be frozen in place at temperatures just below the melting point.

For the large fraction of dopants on the Li site, Li vacancies (V'_{Li}) are needed for charge compensation. The vector between the dopant and V'_{Li} defines an axis for this complex defect, with one V'_{Li} vacancy (axes for dopants with more than one V'_{Li} vacancy can also be defined, but more complicated). This raises a challenging experimental question: can the orientation of these defect axes be controlled and thus optimize the optical properties of the system? In the 1970s, Lüty and co-workers studied a range of compact defects for which the principal defect axis could be rotated using polarized light. For example the axis of the F_A center (an F center adjacent to a Na^+ impurity in KCl, with the defect axis along one of the [100] axes) is easily rotated even at low temperatures [55], and under appropriate conditions most of the F_A centers can be aligned along a specific [100] axis.

The dopant-V'_{Li} defects are even more complex in that the distance between the dopant and Li vacancy can also vary significantly. Dierolf and Sandmann [49] observed several different emission lines for Er ions in LNO, and were able to associate them with different arrangements of the two Li vacancies required for charge compensation. The distribution of V'_{Li} could also be changed by annealing for 5 h at 250 °C; but at room temperature the vacancy distributions were metastable. A similar situation occurs for CaF_2:Yb where interstitial F_i^- defects provide charge compensation for Yb^{3+} dopants. In this system we recently observed several metastable defect configurations [56] that could be changed by a combination of x-ray exposure and annealing. In that case, the changing optical properties appear to depend on the

separation between the Yb and F_i^- defects, and for one configuration an anomalous optical emission was quenched [56].

It appears that metastable configurations of the dopant-compensator defect clearly exist for doped $LiNbO_3$. These ideas likely can be applied to a wide range of doped materials with complex defects both compact defects involving say a neighboring pair of atoms as for the F_A center [55] or for extended defects for which a dopant and charge compensating defect may be well separated, as found for CaF_2:Yb [56]. Although the orientation of compact defects with a well defined axis have been studied extensively, e.g., the F_A center [55] or isovalent off-center defects [57,58], systems with aliovalent dopants, such as the dopants in LNO discussed here, the CaF_2:Yb system [56], and dopants in ferroelectrics [59], are more challenging as the related charge compensating defect can be several lattice spacings away.

If means are found to control the location of the charge compensating Li vacancies in LNO—both separation between dopant and vacancies, and/or the orientation of the axes from the dopant to the vacancies in LNO—it would provide new ways of optimizing the optical behavior of this unusual material.

ACKNOWLEDGMENTS

We thank R. Jackson and M. Valerio for helpful discussions. The experiments were performed at the Stanford Synchrotron Radiation Lightsource (SSRL), which is supported by the U.S. Department of Energy, Office of Science, Office of Basic Energy Sciences under Contract No. DE-AC02-76SF00515.

[1] M. D. Fontana and P. Bourson, Appl. Phys. Rev. **2**, 040602 (2015).
[2] S. Sanna and W. G. Schmidt, J. Phys.: Condens. Matter **29**, 413001 (2017).
[3] S. Nahar, M. F. M. Zain, A. A. H. Kadhum, H. A. Hasan, and M. R. Hasan, Materials **10**, 629 (2017).
[4] L. A. A. García-Cabañes, A. Blázquez-Castro, F. Agulló-López, and M. Carrascosa, Crystals **8**, 65 (2018).
[5] F. Xin, G. Zhang, F. Bo, H. Sun, Y. Kong, J. Xu, T. Volk, and N. M. Rubinina, J. Appl. Phys. **107**, 033113 (2010).
[6] Y. Kong, S. Liu, and J. Xu, Materials **5**, 1954 (2012).
[7] K. Lengyel, Á. Péter, L. Kovács, G. Corradi, L. Pálfalvi, J. Hebling, M. Unferdorben, G. Dravecz, I. Hajdara, Z. Szaller, and K. Polgár, App. Phys. Rev. **2**, 040601 (2015).
[8] J. G. Marques and K. Lorenz, Opt. Eng. **53**, 060901 (2014).
[9] M. Wöhlecke, G. Corradi, and K. Betzler, Appl. Phys. B **63**, 323 (1996).
[10] X. Zhen, Q. Li, and Y. Xu, Cryst. Res. Technol. **41**, 276 (2006).
[11] U. Schlarb and K. Betzler, Phys. Rev. B **50**, 751 (1994).
[12] D.-L. Zhang, C.-X. Qiu, W.-H. Wong, and E. Y.-B. Pun, Mater. Res. Bull. **60**, 771 (2014).
[13] M. Bazzan and C. Sada, Appl. Phys. Rev. **2**, 040603 (2015).
[14] D. Zheng, Y. Kong, S. Liu, J. Yao, L. Zhang, S. Chen, and J. Xu, AIP Adv. **5**, 017132 (2015).
[15] L. Li, Y. Li, and X. Zhao, Phys. Rev. B. **96**, 115118 (2017).
[16] F. Bridges, J. Castillo-Torres, B. Car, S. Medling, and M. Kozina, Phys. Rev. B **85**, 064107 (2012).
[17] F. Bridges, C. MacKeen, and L. Kovács, Phys. Rev. B **94**, 014101 (2016).
[18] R. M. Araujo, K. Lengyel, R. A. Jackson, L. Kovacs, and M. E. G. Valerio, J. Phys.: Condens. Matter **19**, 046211 (2007).
[19] R. M. Araujo, M. E. G. Valerio, and R. A. Jackson, J. Phys.: Condens. Matter **20**, 035201 (2008).
[20] H. Xu, A. Chernatynskiy, D. Lee, S. B. Sinnott, V. Gopalan, V. Dierolf, and S. R. Phillpot, Phys. Rev. B **82**, 184109 (2010).
[21] B. Grabmaier, W. Wersing, and W. Koestler, J. Cryst. Growth **110**, 339 (1991).
[22] R. M. Araujo, M. E. G. Valerio, and R. A. Jackson, Crystals **8**, 123 (2018).
[23] A. A. Kaminskii, *Laser Crystals*, 2nd ed. (Springer, Berlin, 1990), pp. 210–212.
[24] Y. Sun, C. W. Thiel, R. L. Cone, R. W. Equall, and R. L. Hutcheson, J. Lumin. **98**, 281 (2002).
[25] D. Bravo, A. Martín, and F. J. López, Solid State Commun. **112**, 541 (1999).
[26] L. Kovács, L. Kocsor, Z. Szaller, I. Hajdara, G. Dravecz, K. Lengyel, and G. Corradi, Crystals **7**, 230 (2017).
[27] F. A. Kröger and H. J. Vink, Solid State Phys. **3**, 307 (1956).
[28] R. D. Shannon, Acta Crystallogr. Sect. A **32**, 751 (1976).
[29] S. Jang, B. D. White, I. K. Lum, H. Kim, M. A. Tanatar, W. E. Straszheim, R. Prozorov, T. Keiber, F. Bridges, L. Shu, R. E. Baumbach, M. Janoschek, and M. B. Maple, Philos. Mag. **94**, 4219 (2014).
[30] K. Polgár, A. Péter, L. Kovács, G. Corradi, and Z. Szaller, J. Crystal Growth **177**, 211 (1997).
[31] C. H. Booth, R-Space X-ray Absorption Package, 2010, http://lise.lbl.gov/RSXAP/
[32] A. L. Ankudinov and J. J. Rehr, Phys. Rev. B **56**, R1712(R) (1997).
[33] See Supplemental Material at http://link.aps.org/supplemental/10.1103/PhysRevMaterials.2.093602 for details of fitting procedure.
[34] E. A. Stern, Phys. Rev. B **48**, 9825 (1993).
[35] L. Downward, C. H. Booth, W. W. Lukens, and F. Bridges, AIP Conf. Proc. **882**, 129 (2007).
[36] I. Baumann, R. Brinkmann, M. Dinand, W. Sohler, L. Beckers, C. Buchal, M. Fleuster, H. Holzbrecher, H. Paulus, K.-H. Müller, T. Gog, G. Materlik, O. Witte, H. Stolz, and W. von der Osten, Appl. Phys. A **64**, 33 (1997).
[37] C. Prieto, C. Zaldo, P. Fessler, H. Dexpert, J. A. Sanz-Garcia, and E. Dieguez, Phys. Rev. B **43**, 2594 (1991).
[38] C. Zaldo and C. Prieto, Ferroelectrics **134**, 47 (1992).
[39] C. Prieto and C. Zaldo, J. Phys.: Condens. Matter **6**, L677 (1994).
[40] J. J. Rehr, R. C. Albers, and S. I. Zabinsky, Phys. Rev. Lett. **69**, 3397 (1992).
[41] S. I. Zabinsky, J. J. Rehr, A. L. Ankudinov, R. C. Albers, and M. J. Eller, Phys. Rev. B **52**, 2995 (1995).

[42] A. McKale, B. Veal, A. Paulikas, S.-K. Chan, and G. Knapp, J. Am. Chem. Soc. **110**, 3763 (1988).
[43] J. Rehr, J. M. de Leon, S. Zabinsky, and R. Albers, J. Am. Chem. Soc. **113**, 5135 (1991).
[44] Y. Kong, J. Deng, W. Zhang, J. Wen, G. Zhang, and H. Wang, Phys. Lett. A **196**, 128 (1994).
[45] B. Hauer, R. Vianden, J. G. Marques, N. P. Barradas, J. G. Correia, A. A. Melo, J. C. Soares, F. Agulló-López, and E. Dieguez, Phys. Rev. B **51**, 6208 (1995).
[46] L. Rebouta, M. da Silva, J. Soares, J. Sanz-García, E. Dieguez, and F. Agulló-López, Nucl. Instrum. Methods Phys. Res. B **64**, 189 (1992).
[47] M. G. Th. Gog and G. Materlik, Phys. Lett. A **181**, 417 (1993).
[48] V. Dierolf and M. Koerdt, Phys. Rev. B **61**, 8043 (2000).
[49] V. Dierolf and C. Sandmann, J. Lumin. **125**, 67 (2007).
[50] T. P. Th. Nolte and J.-M. Spaeth, Solid State Commun. **104**, 535 (1997).
[51] R. Hammoum, M. Fontana, M. Gilliot, P. Bourson, and E. Kokanyan, Solid State Commun. **149**, 1967 (2009).
[52] L. Kovács, Z. Szaller, K. Lengyel, and G. Corradi, Opt. Mater. **37**, 55 (2014).
[53] J. G. Marques, A. Kling, J. Soares, L. Rebouta, M. da Silva, E. Diéguez, and F. Agulló-López, Nucl. Instrum. Methods Phys. Res. B **136–138**, 431 (1998).
[54] H. Xu, D. Lee, S. Sinnott, V. Dierolf, V. Gopalan, and S. Phillpot, J. Phys.: Condens. Matter **22**, 135002 (2010).
[55] H. Blume, T. Bader, and F. Lüty, Opt. Commun. **12**, 147 (1974).
[56] C. MacKeen, F. Bridges, L. Seijo, Z. Barandiarán, M. Kozina, A. Mehta, M. F. Reid, and J.-P. R. Wells, J. Phys. Chem. C **121**, 28435 (2017).
[57] W. M. Kelly and F. Bridges, Phys. Rev. B. **18**, 4606 (1978).
[58] B. Y. Price, G. Hardal, M. Açıkgöz, S. Repp, and E. Erdem, J. Appl. Phys. **118**, 175705 (2015).
[59] E. Erdem, R. Böttcher, H.-J. Gläsel, and E. Hartmann, Magn. Reson. Chem. **43**, S174 (2005).